Electronic Supplementary Information

Substituent effect and wavelength dependence of the photoinduced Ru-O homolysis in the $[Ru(bpy)_2(py\text{-}SO_3)]^+$–type complexes

*Yue Zheng,[ab] Qian-Xiong Zhou,[*a] Yang-Yang Zhang,[ab] Chao Li,[a] Yuan-Jun Hou[a] and Xue-Song Wang [*a]*

[a]Key Laboratory of Photochemical Conversion and Optoelectronic Materials, Technical Institute of Physics and Chemistry,
Chinese Academy of Sciences, Beijing 100190, P. R. China. Fax: +86-10-62564049; Tel: +86-10-82543592; E-mail:xswang@mail.ipc.ac.cn (X. Wang); zhouqianxiong@mail.ipc.ac.cn (Q. Zhou).
[b]Graduate School of Chinese Academy of Sciences, Beijing 100049, P. R. China.

Instruments and methods

^{1}H NMR spectra were obtained on a Bruker DMX-400 MHz. High-resolution ESI-MS spectra were determined on a Brucker APEX IV (7.0T) FT_MS. Elemental analysis was performed on an Elementar Vario EL instrument. UV-vis absorption and 77 K emission spectra were recorded on a Shimadzu UV-1601 spectrophotometer and Hitachi F-4600 fluorescence spectrophotometer, respectively.

Oil/water partition coefficients (log $P_{O/W}$) were determined at room temperature following a reported method.[1] Typically, 1 mL of aqueous solutions of the examined complexes (25 μM) were mixed with 1 mL of *n*-octanol and sonicated for 30 min. After separation by centrifugation, the amounts of complex in each phase were quantified by the absorbance at absorption maximum of the examined complex. The results were the average of three independent measurements.

The EPR spectra were measured on a Bruker ESP-300E spectrometer at 9.8 GHz, X-band, with 100 Hz field modulation. Samples were injected quantitatively into quartz capillaries, purged with argon for 20 min in the dark, and illuminated in the cavity of the EPR spectrometer with a Nd:YAG laser at 355 nm or 532 nm (5-6 ns of pulse width, 10 Hz of repetition frequency, 30 mJ/pulse energy).

The redox potentials were measured on an EG&G Model283 Potentiostat/Galvanostat in a three-electrode cell with a glassy carbon working electrode, a Pt counter electrode, and a saturated calomel electrode (SCE) as reference. The cyclic voltammetry was conducted at a scan rate of 50 mV s^{-1} in Ar-saturated, anhydrous CH_3CN containing 0.1 M tetra-*n*-butylammonium hexafluoro-phosphate as the supporting electrolyte.

All calculations were performed with the Gaussian 09[2] (G09) program package 3 employing the density functional theory (DFT) method with Becke's three-parameter hybrid functional and LeeYang-Parr's gradient corrected correlation functional (B3LYP).[3] The SDD basis set[4] and effective core potential were used for the Ru atom, and the 6-31 G* basis set was applied for H, C, N, O and S.[5] The ground-state geometry of **1-4** was optimized in H_2O using the conductive polarizable continuum model (CPCM), and frequency calculation was also performed to verify the optimized structure to be at an energy minimum. Time-dependent density functional theory (TD-DFT) calculation was used to characterize the properties of singlet and triplet excited states, and the CPCM model with H_2O as solvent was applied to the solvent effect.

The photoinduced ligand dissociation experiments were carried out under irradiation of a 15 W LED lamp (λ = 470 nm).

Supercoiled pBR322 plasmid DNA was used to study DNA photodamage. 40 μL of pBR322 plasmid DNA (40 μg/mL) was incubated with a complex dosed from 0 to 20 or 40 μM. The mixture was irradiated with laser (355 nm, 90 mW) or LED lamp (470 nm, 15 W) for 8 minutes.

After irradiation and incubation at room temperature for 2 h, 10 μL loading buffer was added. 10 μL of sample was taken for agarose gel (1%) electrophoresis (in Tris-acetic acid-EDTA buffer, pH (8.0) at 5 V/cm for 1.5 h. The gel was stained with EB (1 mg/L in H_2O) for 0.5 h and then analyzed using a Gel Doc XR system (Bio-Rad).

Anaerobic conditions were obtained by bubbling the solutions with high-purity argon for 20 min. All measurements were carried out at room temperature.

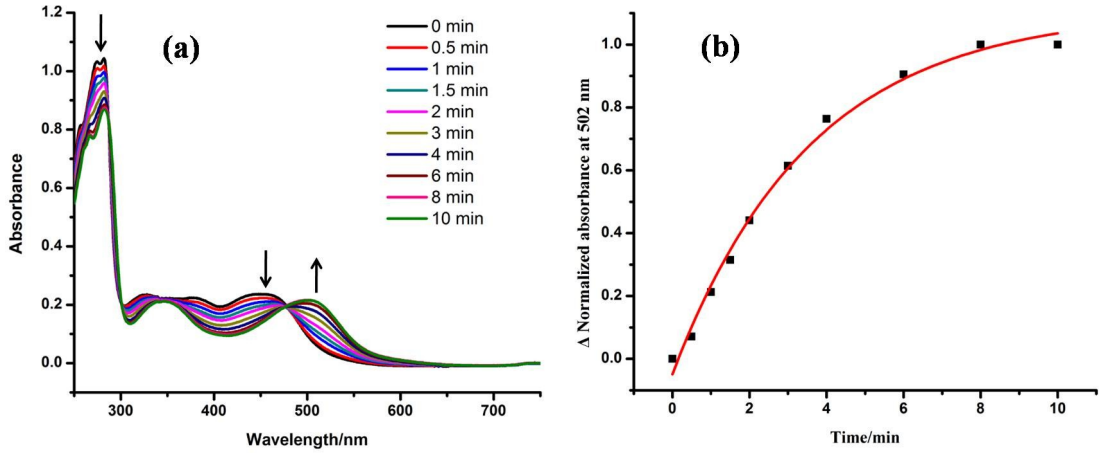

Figure S1. (a) Absorption spectra changes of **1** (25 μM) in Ar-saturated H_2O upon irradiation (470 nm). (b) Absorbance changes at 502 nm as a function of irradiation time.

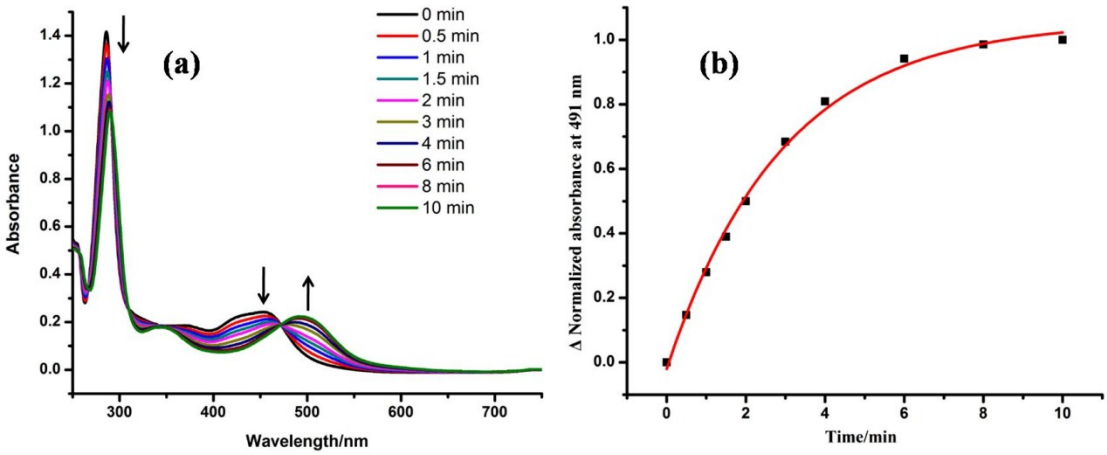

Figure S2. (a) Absorption spectra changes of **2** (25 μM) in Ar-saturated H_2O upon irradiation (470 nm). (b) Absorbance changes at 491 nm as a function of irradiation time.

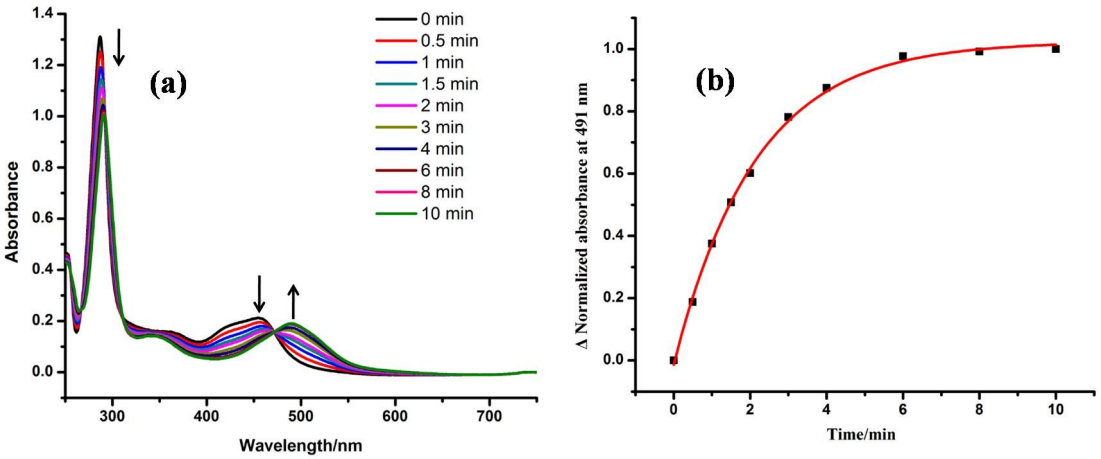

Figure S3. (a) Absorption spectra changes of **3** (25 μM) in Ar-saturated H_2O upon irradiation (470 nm). (b) Absorbance changes at 491 nm as a function of irradiation time.

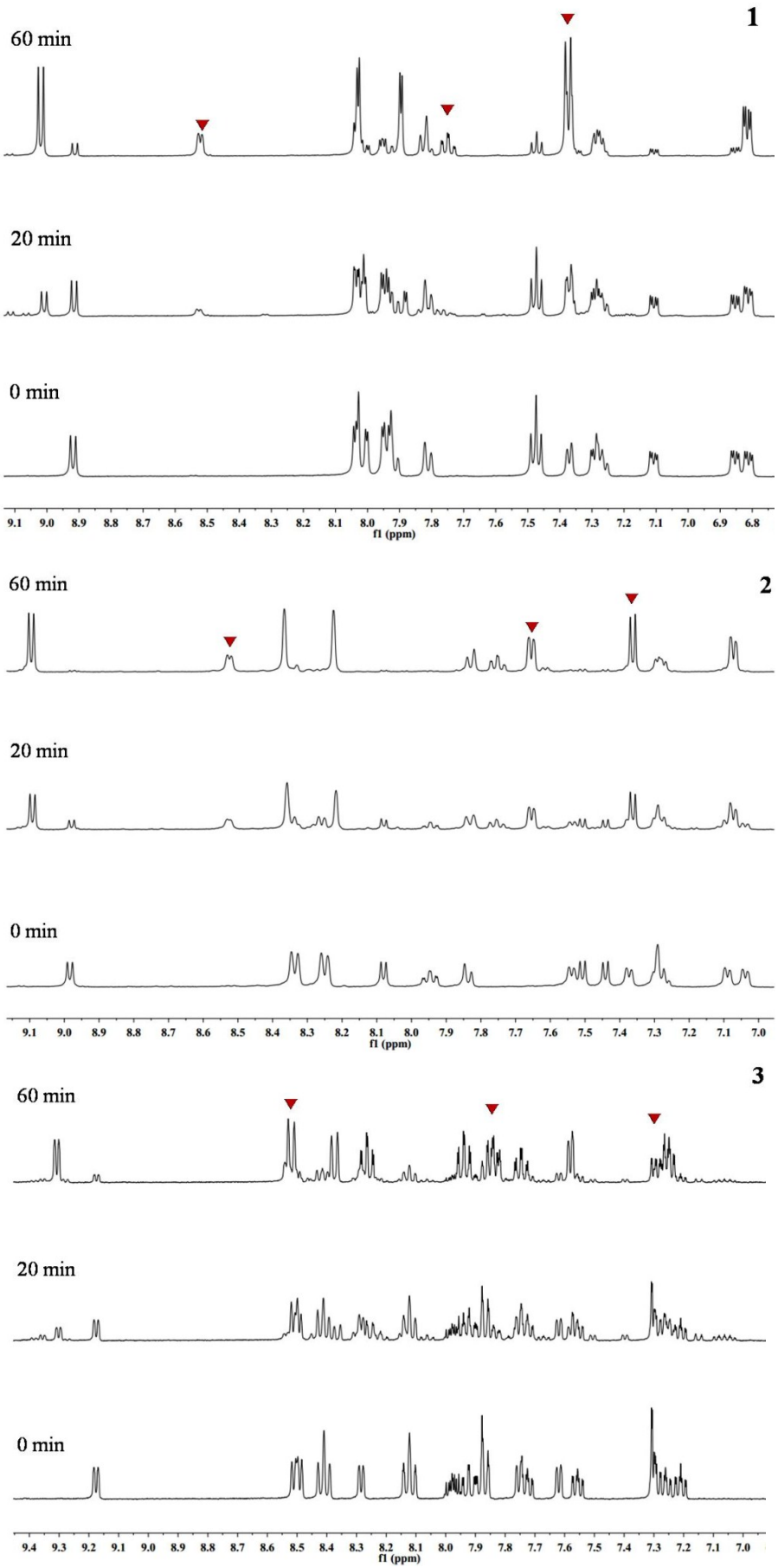
1
60 min
20 min
0 min
9.1 9.0 8.9 8.8 8.7 8.6 8.5 8.4 8.3 8.2 8.1 8.0 7.9 7.8 7.7 7.6 7.5 7.4 7.3 7.2 7.1 7.0 6.9 6.8
f1 (ppm)
2
60 min
20 min
0 min
9.1 9.0 8.9 8.8 8.7 8.6 8.5 8.4 8.3 8.2 8.1 8.0 7.9 7.8 7.7 7.6 7.5 7.4 7.3 7.2 7.1 7.0
f1 (ppm)
3
60 min
20 min
0 min
9.4 9.3 9.2 9.1 9.0 8.9 8.8 8.7 8.6 8.5 8.4 8.3 8.2 8.1 8.0 7.9 7.8 7.7 7.6 7.5 7.4 7.3 7.2 7.1 7.0
f1 (ppm)

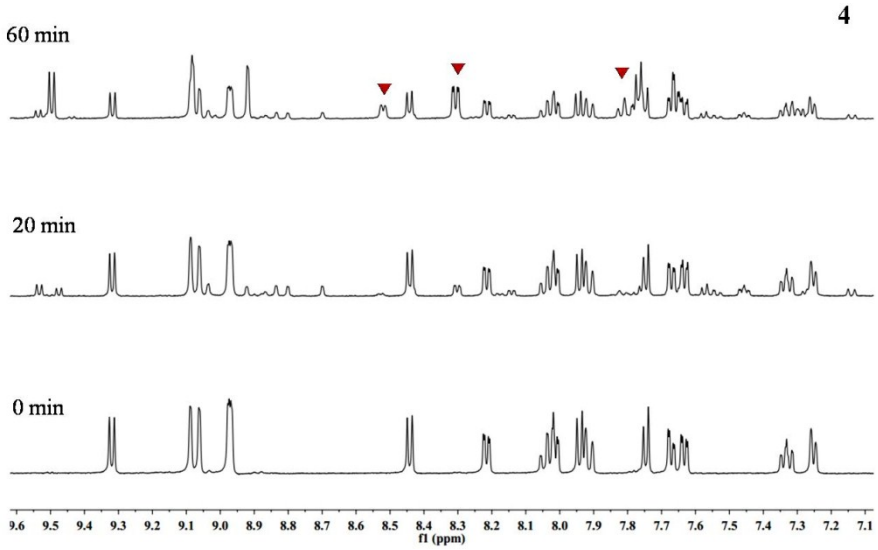

Figure S4. ^{1}H NMR spectra changes of **1-4** in Ar-saturated CD_3CN before and after irradiation at 470 nm for 20 and 60 min. The red triangles indicate the chemical shifts from the free ligand of py-SO_3.

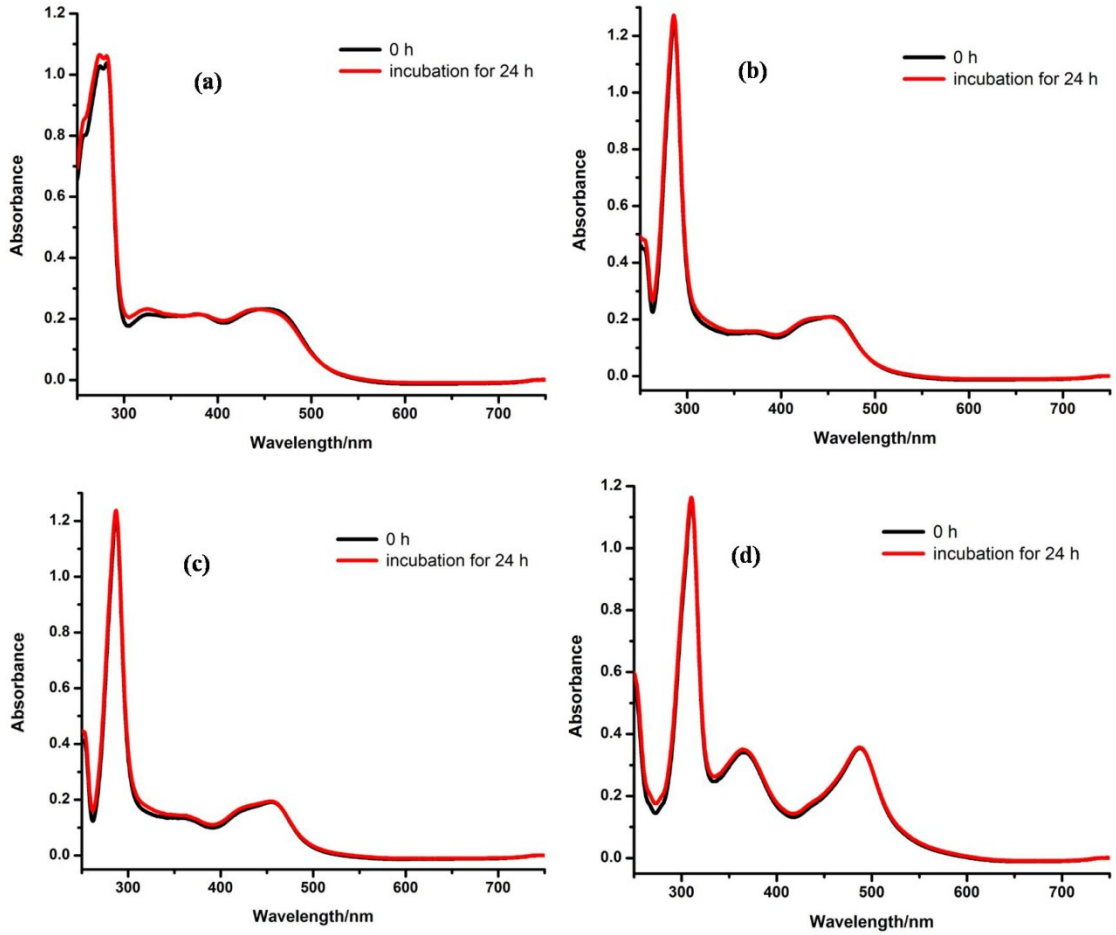

Figure S5. Absorption spectra of **1-4** (a-d, 25 μM) in aqueous solutions either freshly prepared or after standing for 24 h in the dark.

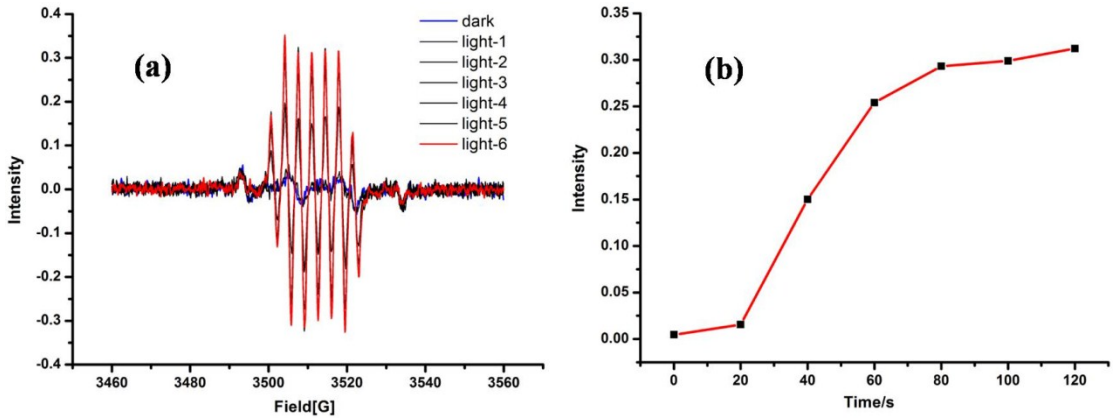

Figure S6. (a) EPR signals obtained upon laser irradiation (355 nm) of an Ar-saturated CH_3CN solution of **1** and DMPO (50 mM). (b) EPR signal intensity changes as a function of irradiation time.

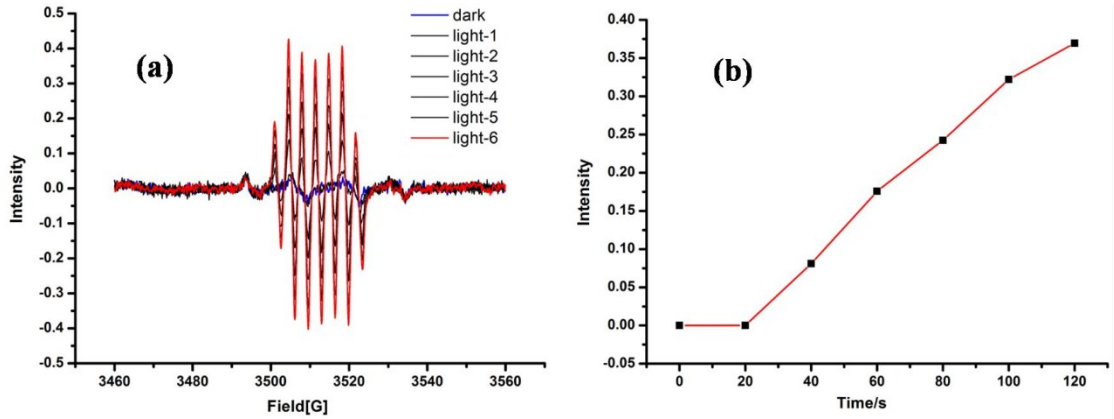

Figure S7. (a) EPR signals obtained upon laser irradiation (355 nm) of an Ar-saturated CH_3CN solution of **2** and DMPO (50 mM). (b) EPR signal intensity changes as a function of irradiation time.

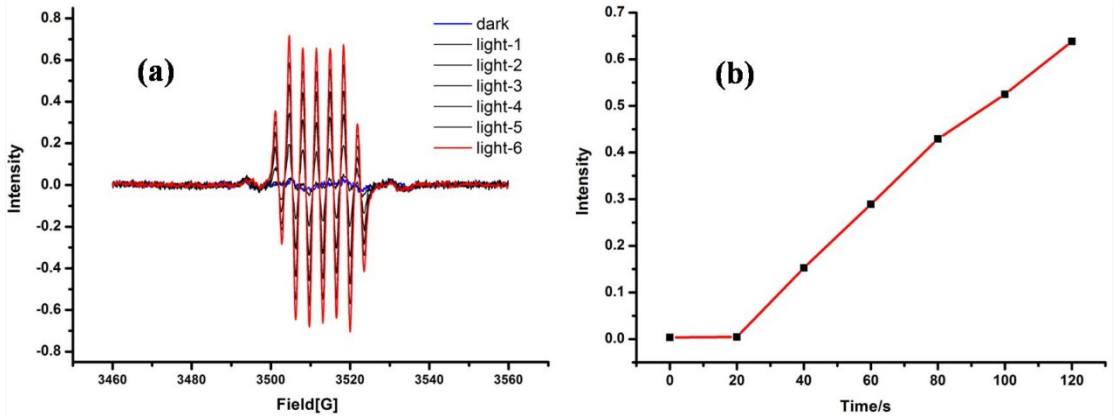

Figure S8. (a) EPR signals obtained upon laser irradiation (355 nm) of an Ar-saturated CH_3CN solution of **3** and DMPO (50 mM). (b) EPR signal intensity changes as a function of irradiation time.

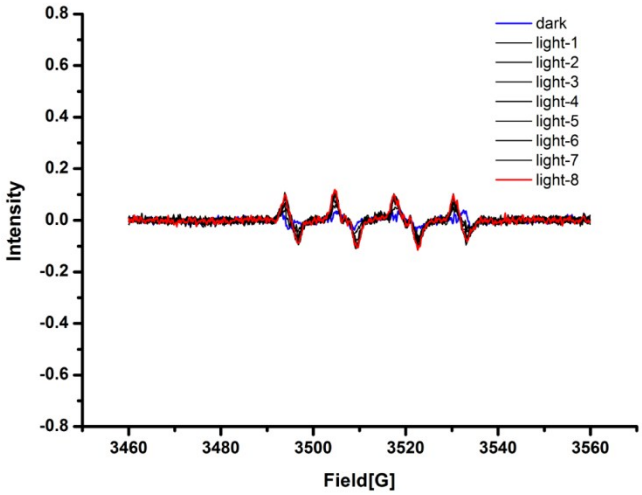

Figure S9. EPR signals obtained upon laser irradiation (532 nm) of an Ar-saturated CH_3CN solution of **4** and DMPO (50 mM).

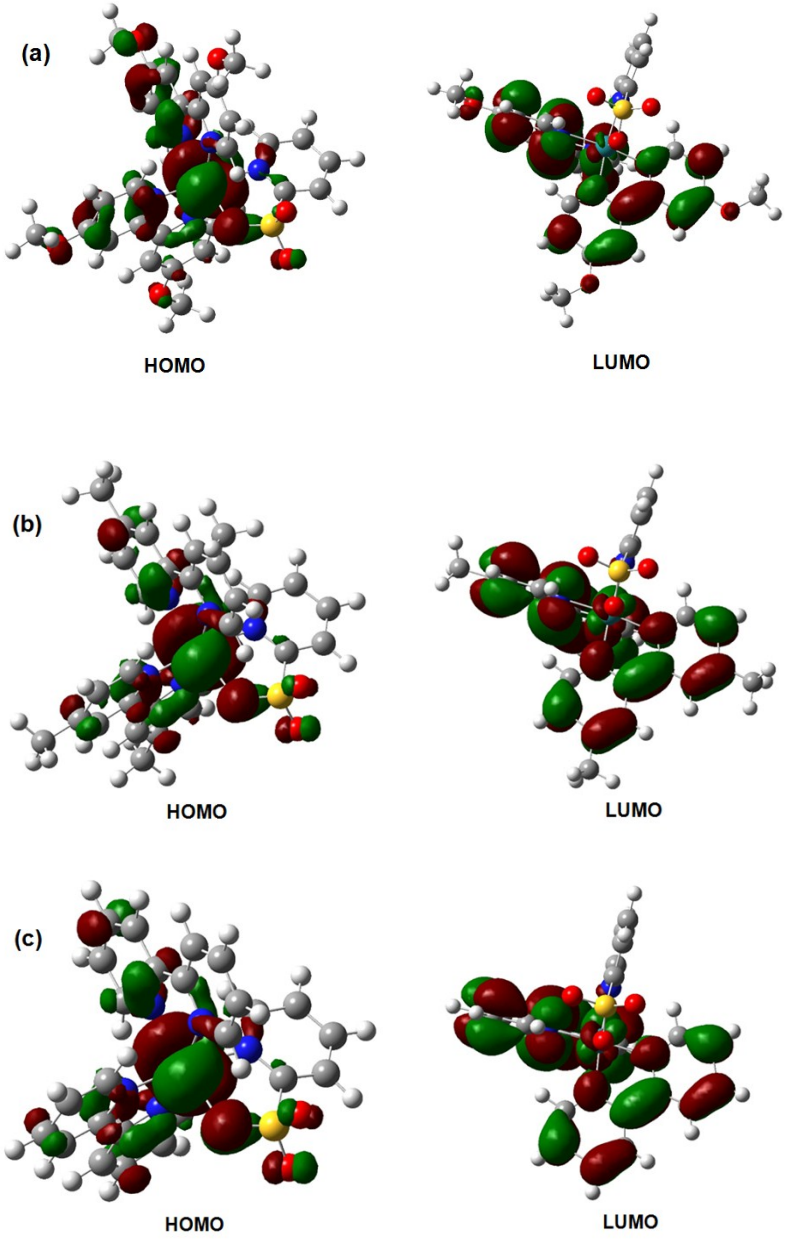

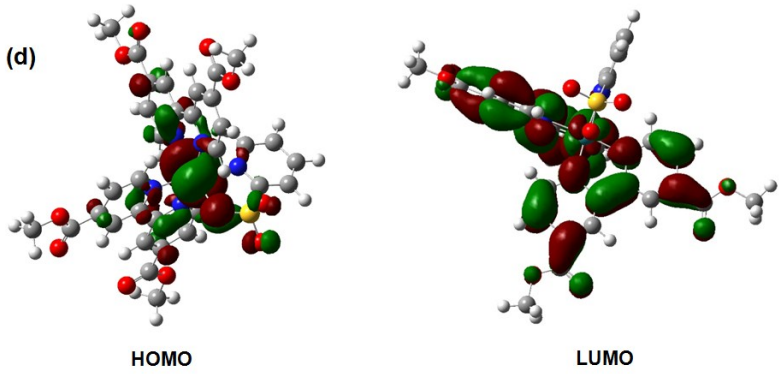

Figure S10. Calculated HOMO and LUMO orbitals of **1** (a), **2** (b), **3** (c), and **4** (d).

Table S1. Selected triplet excited states of **1** obtained from TD-DFT calculations (H = HOMO, L = LUMO).

Triplet excited state	**Energy (eV)**	**Wavelength (nm)**	**Oscillator strength (f)**	**Calculated transitions and orbital contributions**
1	2.3441	528.92	0.000	H→L (61%) H→L+3(3%) H→L+8(26%)
2	2.3956	517.54	0.000	H→L+1(82%) H→L+5(3%) H→L+8(6%)
4	2.5128	493.40	0.000	H-2→L (3%) H-2→L+1(4%) H-1→L+1(20%) H→L (18%) H→L+1(7%) H→L+8(38%)
11	2.9178	424.92	0.000	H-2→L (7%) H-2→L+1(3%) H-2→L+8(75%) H-2→L+9(6%)
38	4.3355	285.97	0.000	H-14→L+2(6%) **H-9→L+2(26%) H-9→L+4(3%)** H-8→L+2(46%) H-8→L+4(6%)

Table S2. Selected triplet excited states of **2** obtained from TD-DFT calculations (H = HOMO, L = LUMO).

Triplet excited state	**Energy (eV)**	**Wavelength (nm)**	**Oscillator strength (f)**	**Calculated transitions and orbital contributions**
1	2.2741	545.19	0.000	H-1→L+1(3%) H→L (72%) H→L+1(8%) H→L+8(8%)
2	2.3009	538.84	0.000	H→L (7%) H→L+1(79%) H→L+8(4%)
6	2.5586	484.58	0.000	H-2→L+1(3%) H-1→L (8%) H-1→L+1(3%) H→L (14%) H→L+8(65%)
12	3.0309	409.07	0.000	H-2→L+12(5%) H-1→L+8(6%) H→L+9(17%) H→L+11(3%) H→L+12(59%)
40	4.3405	285.64	0.000	H-11→L (3%) H-9→L+1(3%) H-8→L+1 (4%) H-7→L (8%) H-7→L+1(10%) **H-5→L (5%)** **H-5→L+1(4%)** H-4→L+1(24%) H-3→ L (7%)

Table S3. Selected triplet excited states of **3** obtained from TD-DFT calculations (H = HOMO, L = LUMO).

Triplet excited state	Energy (eV)	Wavelength (nm)	Oscillator strength (f)	Calculated transitions and orbital contributions
1	2.2839	542.87	0.000	H-1→L+1(3%) H→L (63%) H→L+1(18%) H→L+8(5%)
2	2.3124	536.17	0.000	H→L (17%) H→L+1(70%) H→L+8(5%)
6	2.5862	479.41	0.000	H-2→L+1(3%) H-1→L (5%) H→L (13%), H→L+8(72%)
11	3.0546	405.89	0.000	H-2→L+11(3%) H-1→L+8(6%) H→L+2(3%) H→L+9(32%) H→L+11(40%)
41	4.4399	279.25	0.000	H-12→L (6%) H-12→L+1(5%) H-11→L+1 (6%) **H-5→L (16%)** **H-5→L+1(11%)** H-4→ L+4(5%) H-4→L+7(3%) H-3→L+4(6%) H-3→ L+5(5%) H-3→L+7(8%)

Table S4. Selected triplet excited states of **4** obtained from TD-DFT calculations (H = HOMO, L = LUMO).

Triplet excited state	Energy (eV)	Wavelength (nm)	Oscillator strength (f)	Calculated transitions and orbital contributions
1	2.0586	602.27	0.000	H-2→L+1(3%) H-1→L+1(6%) H→L (42%) H→L+1(40%)
2	2.0964	591.43	0.000	H→L (45%) H→L+1(47%)
7	2.6290	471.59	0.000	H→L+8(90%)
8	2.8735	431.47	0.000	H-1→L+8(74%) H→L+3 (7%) H→L+11(8%)
41	4.0435	306.63	0.000	H-6→L+7(3%) **H-5→L (13%)** **H-5→L+1(7%)** H-4→L (11%) H-4→L+1(3%) H-3→L+1(16%)

Table S5. Calculated Oxygen Character in the Selected Molecular Orbitals of **1-4**.

	1	**2**	**3**	**4**
HOMO	3.19%	4.14%	4.76%	6.00%
HOMO-1	4.10%	4.02%	3.95%	4.16%
HOMO-2	0.11%	0.40%	0.64%	0.75%
HOMO-3	0.09%	0.58%	0.69%	1.51%
HOMO-4	0.86%	0.99%	0.10%	0.15%
HOMO-5	8.07%	20.18%	18.88%	14.43%
HOMO-9	7.38%	---	---	---

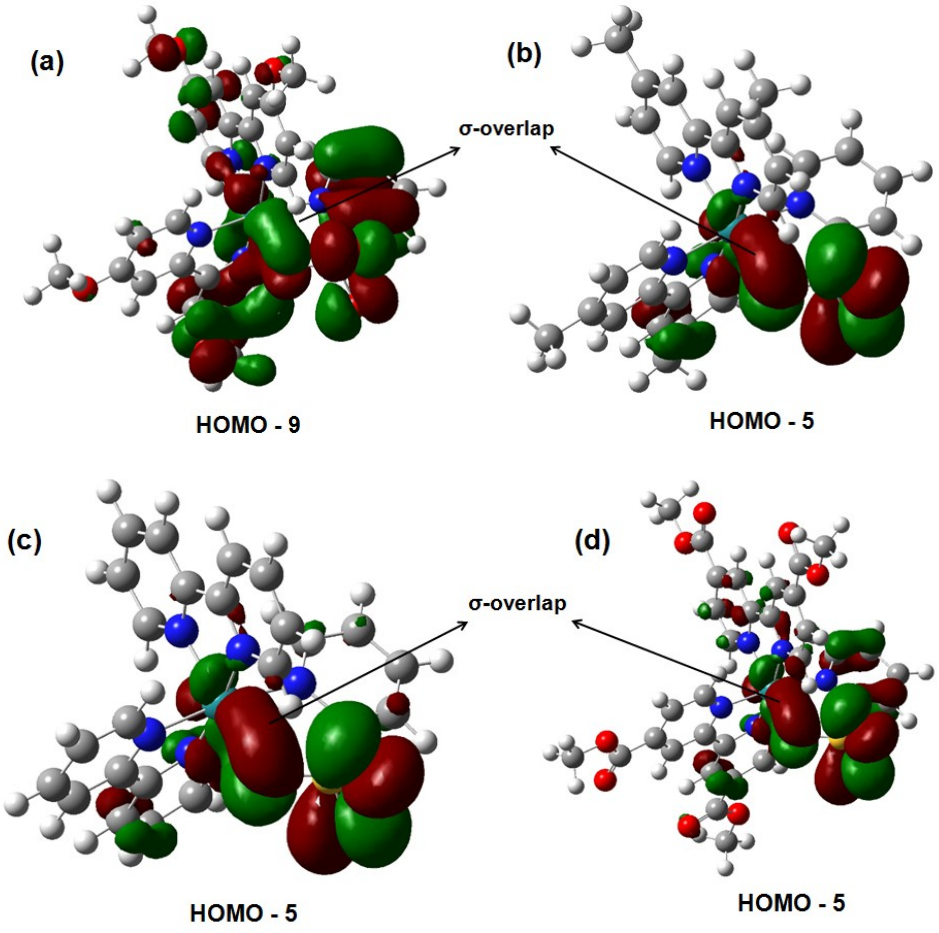

Figure S11. σ(Ru-O) orbitals of **1** (a), **2** (b), **3** (c) and **4** (d).

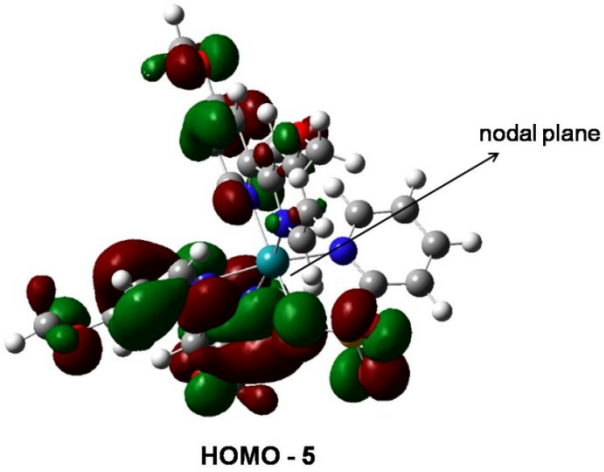

Figure S12. HOMO-5 orbital of **1**.

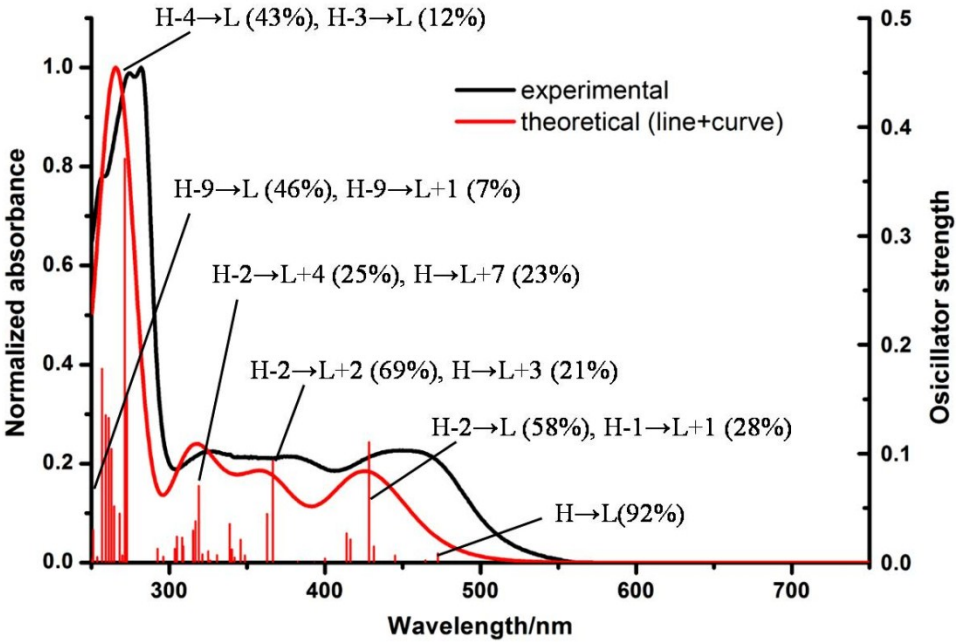

Figure S13. Normalized experimental and theoretical spectra of **1** in H_2O. MO contributions and transition energies were calculated using TD-DFT and only select contributions greater than 5% are assigned (H = HOMO, L = LUMO).

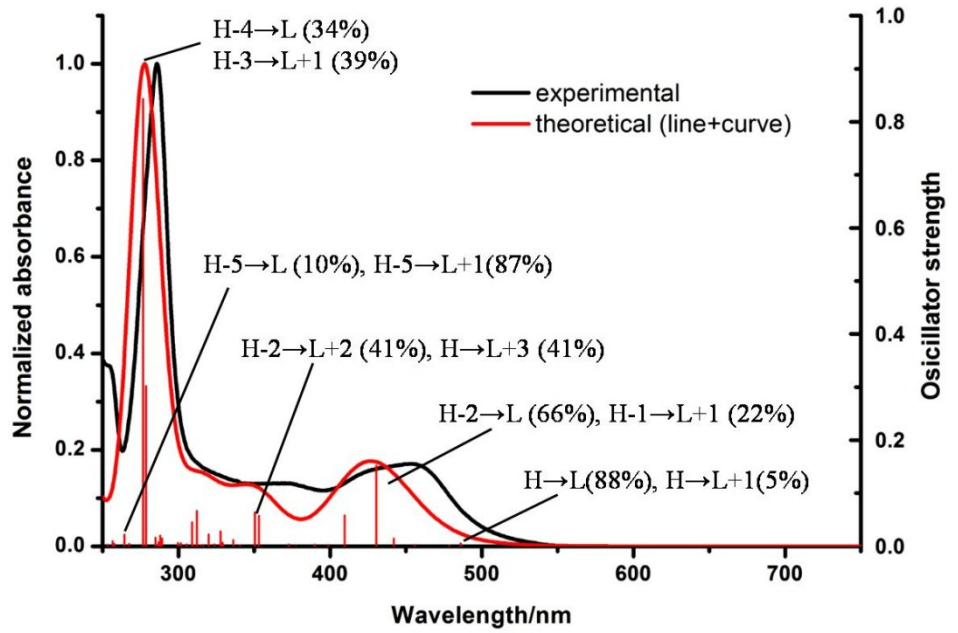

Figure S14. Normalized experimental and theoretical spectra of **2** in H_2O. MO contributions and transition energies were calculated using TD-DFT and only select contributions greater than 5% are assigned (H = HOMO, L = LUMO).

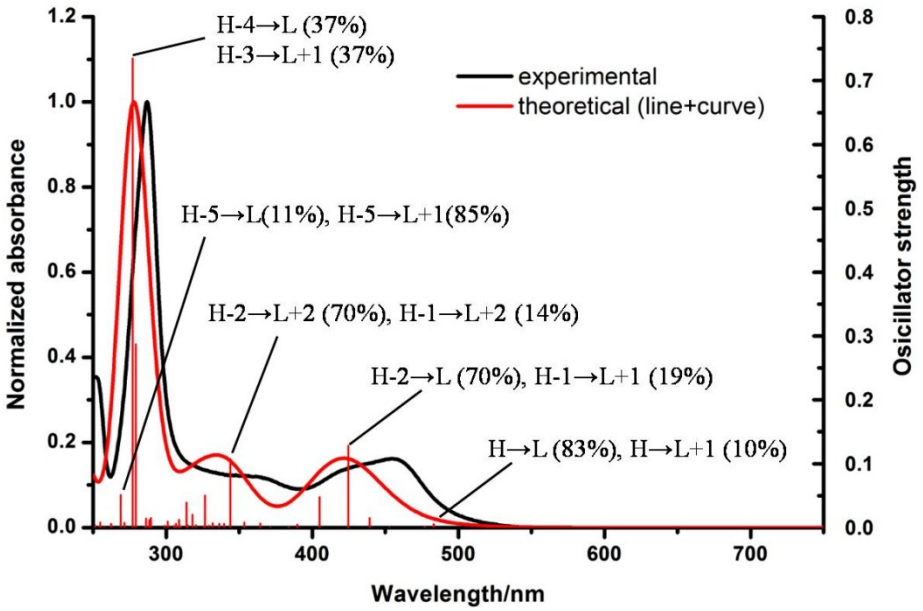

Figure S15. Normalized experimental and theoretical spectra of **3** in H_2O. MO contributions and transition energies were calculated using TD-DFT and only select contributions greater than 5% are assigned (H = HOMO, L = LUMO).

Table S6. Selected TD-DFT singlet excited states of **1** and the transitions associated with these states in H_2O (H = HOMO, L = LUMO).

Singlet excited state	**Energy (eV)**	**Wavelength (nm)**	**Oscillator strength (f)**	**Calculated transitions and orbital contributions**
1	2.6235	472.58	0.0085	**H→L (92%)**
5	2.8949	428.29	0.1105	**H-2→L (58%)** H-1→L (10%) H-1→L+1 (28%)
11	3.3819	366.61	0.0940	H-2→L+2 (69%) H-1→L+2 (3%) H→L+3 (21%)
40	4.8863	253.74	0.0053	H-9→L+2(6%) H-6→L+2(18%) H-5→L+2(36%) H-4→L+2(19%) H-3→L+2(13%)
44	4.9964	248.15	0.0381	H-10→L(3%) **H-9→L(46%)** **H-9→L+1(7%)** H-4→L+1(30%)

Table S7. Selected TD-DFT singlet excited states of **2** and the transitions associated with these states in H_2O (H = HOMO, L = LUMO).

Singlet excited state	Energy (eV)	Wavelength (nm)	Oscillator strength (f)	Calculated transitions and orbital contributions
1	2.5514	485.94	0.0058	**H→L(88%)** H→L+1(5%)
5	2.8800	430.51	0.1528	**H-2→L (66%)** H-1→L (8%) H-1→L+1 (22%)
12	3.5393	350.31	0.0641	H-2→L+2 (41%) H-1→L+2 (6%) H→L+3 (41%)
35	4.6344	267.53	0.0051	H-5→L(86%) H-5→L+1(9%)
36	4.6903	264.34	0.0222	**H-5→L(10%)** **H-5→L+1(87%)**

Table S8. Selected TD-DFT singlet excited states of **3** and the transitions associated with these states in H_2O (H = HOMO, L = LUMO).

Singlet excited state	Energy (eV)	Wavelength (nm)	Oscillator strength (f)	Calculated transitions and orbital contributions
1	2.5661	483.15	0.0056	**H→L(83%)** H→L+1(10%)
5	2.9193	424.70	0.1285	**H-2→L (70%)** H-1→L (5%) H-1→L+1 (19%)
12	3.6047	343.95	0.1074	H-2→L+2 (70%) H-1→L+2 (14%) H-1→L+3 (4%) H→L+6 (3%)
35	4.5679	271.43	0.0076	H-5→L(85%) H-5→L+1(10%)
36	4.6120	268.83	0.0513	**H-5→L(11%)** **H-5→L+1(85%)**

Table S9. Selected TD-DFT singlet excited states of **4** and the transitions associated with these states in H_2O (H = HOMO, L = LUMO).

Singlet excited state	Energy (eV)	Wavelength (nm)	Oscillator strength (f)	Calculated transitions and orbital contributions
1	2.3404	529.76	0.0102	**H→L (83%)** H→L+1(10%)
5	2.7124	457.10	0.2160	**H-2→L (64%)** H-1→L (10%) H-1→L+1 (22%)
9	3.2799	378.02	0.1300	H-1→L+1 (3%) **H-1→L+2 (21%)** H-1→L+3 (7%) H→L+2 (4%) **H→L+3 (49%)** H→L+8(9%)
24	3.9585	313.21	0.0254	H-5→L (3%) H-2→L+6(56%) H-1→L+5 (10%) H→L+3 (3%) H→L+7 (4%) H→L+11 (4%)
32	4.1811	296.53	0.0054	H-6→L (3%) H-5→L (83%) H-1→L+7(6%)
33	4.2353	292.74	0.0695	**H-5→L (5%)** **H-5→L+1(61%)** H-1→L+7(26%)

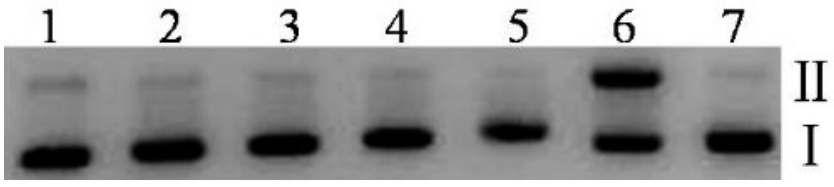

Figure S16. Agarose gel electrophoresis pattern of pBR322 DNA (100 mM in base pairs) in Ar-saturated Tris–EDTA (5 mM, pH = 7.5) upon irradiation (470 nm) for 8 min in the presence of varied concentrations of **4**. Lane 1, DNA alone; lane 2, 5 μM; lane 3, 10 μM; lane 4, 20 μM; lane 5, 40 μM; lane 6, $[Ru(bpy)_3]^{2+}$ (100 μM), air-saturated; lane 7, 50 μM (dark). I and II denote supercoiled circular and nicked circular plasmid DNA, respectively.

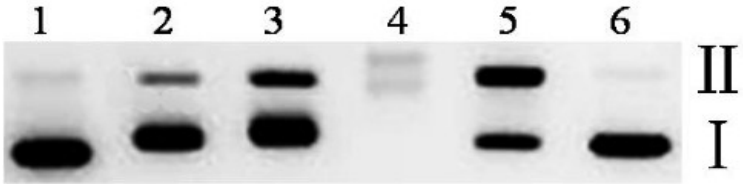

Figure S17. Agarose gel electrophoresis pattern of pBR322 DNA (100 mM in base pairs) in Ar-saturated Tris–EDTA (5 mM, pH = 7.5) upon irradiation (355 nm) for 8 min in the presence of varied concentrations of **3**. Lane 1, DNA alone; lane 2, 5 μM; lane 3, 10 μM; lane 4, 20 μM; lane 5, $[Ru(bpy)_3]^{2+}$ (100 μM), (air-saturated, 470 nm LED, 15W, 15 min); lane 6, 50 μM (dark). I and II denote supercoiled circular and nicked circular plasmid DNA, respectively.

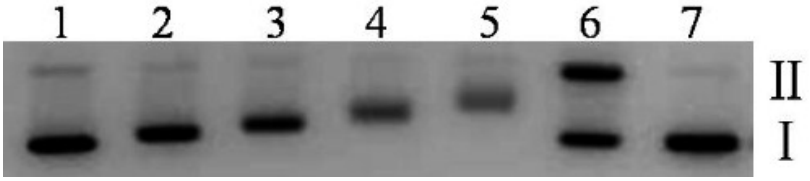

Figure S18. Agarose gel electrophoresis pattern of pBR322 DNA (100 mM in base pairs) in Ar-saturated Tris-EDTA (5 mM, pH = 7.5) upon irradiation (470 nm) for 8 min in the presence of varied concentrations of **3**. Lane 1, DNA alone; lane 2, 5 μM; lane 3, 10 μM; lane 4, 20μM; lane 5, 40 μM; lane 6, $[Ru(bpy)_3]^{2+}$ (100 μM), air-saturated; lane 7, 50 μM (dark). I and II denote supercoiled circular and nicked circular plasmid DNA, respectively.

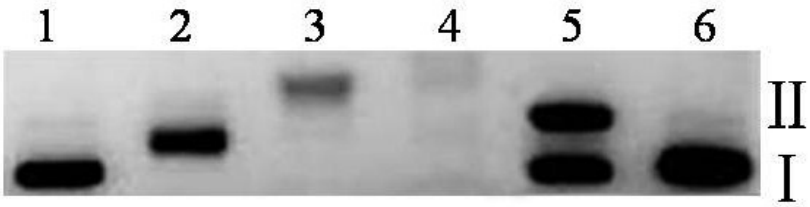

Figure S19. Agarose gel electrophoresis pattern of pBR322 DNA (100 mM in base pairs) in Ar-saturated Tris–EDTA (5 mM, pH = 7.5) upon irradiation (355 nm) for 8 min in the presence of varied concentrations of **1**. Lane 1, DNA alone; lane 2, 5 μM; lane 3, 10 μM; lane 4, 20 μM; lane 5, $[Ru(bpy)_3]^{2+}$ (100 μM), (air-saturated, 470 nm LED, 15 W, 15 min); lane 6, 50 μM (dark). I and II denote supercoiled circular and nicked circular plasmid DNA, respectively.

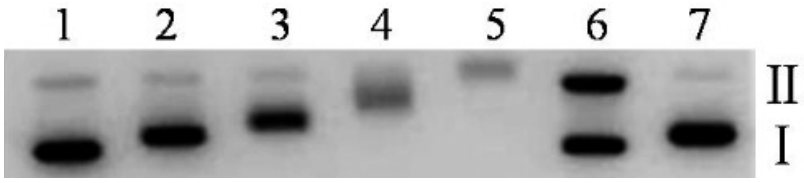

Figure S20. Agarose gel electrophoresis pattern of pBR322 DNA (100 mM in base pairs) in Ar-saturated Tris–EDTA (5 mM, pH = 7.5) upon irradiation (470 nm) for 8 min in the presence of varied concentrations of **1**. Lane 1, DNA alone; lane 2, 5 μM; lane 3, 10 μM; lane 4, 20 μM; lane 5, 40 μM; lane 6, $[Ru(bpy)_3]^{2+}$ (100 μM), air-saturated; lane 7, 50 μM (dark). I and II denote supercoiled circular and nicked circular plasmid DNA, respectively.

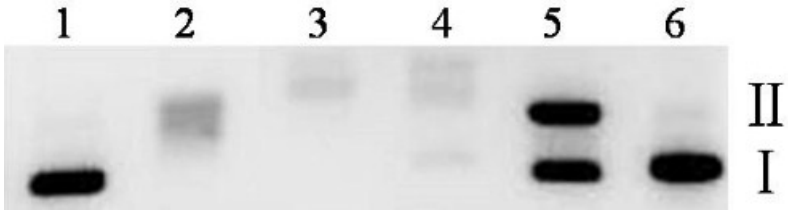

Figure S21. Agarose gel electrophoresis pattern of pBR322 DNA (100 mM in base pairs) in Ar-saturated Tris–EDTA (5 mM, pH = 7.5) upon irradiation (355 nm) for 8 min in the presence of varied concentrations of **2**. Lane 1, DNA alone; lane 2, 5 μM; lane 3, 10 μM; lane 4, 20 μM; lane 5, $[Ru(bpy)_3]^{2+}$ (100 μM), (air-saturated, 470 nm LED, 15 W, 15 min); lane 6, 50 μM (dark). I and II denote supercoiled circular and nicked circular plasmid DNA, respectively.

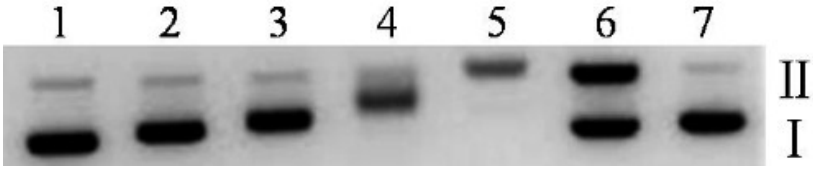

Figure S22. Agarose gel electrophoresis pattern of pBR322 DNA (100 mM in base pairs) in Ar-saturated Tris–EDTA (5 mM, pH = 7.5) upon irradiation (470 nm) for 8 min in the presence of varied concentrations of **2**. Lane 1, DNA alone; lane 2, 5 μM; lane 3, 10 μM; lane 4, 20 μM; lane 5, 40 μM; lane 6, $[Ru(bpy)_3]^{2+}$ (100 μM), air-saturated; lane 7, 50 μM (dark). I and II denote supercoiled circular and nicked circular plasmid DNA, respectively.

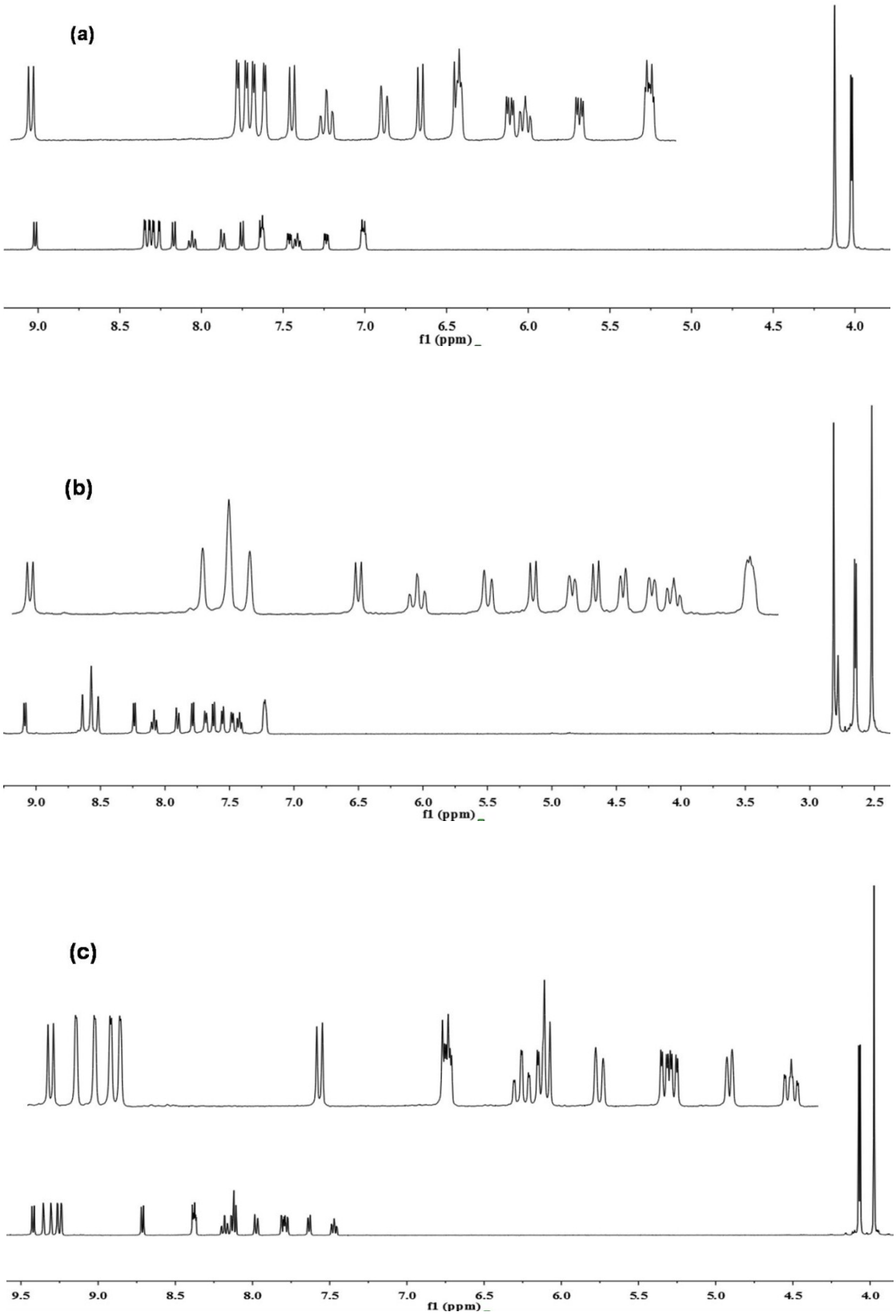

Figure S23. ^{1}H NMR spectra of **1** (a), **2** (b), and **4** (c) in $(CD_3)_2CO$.

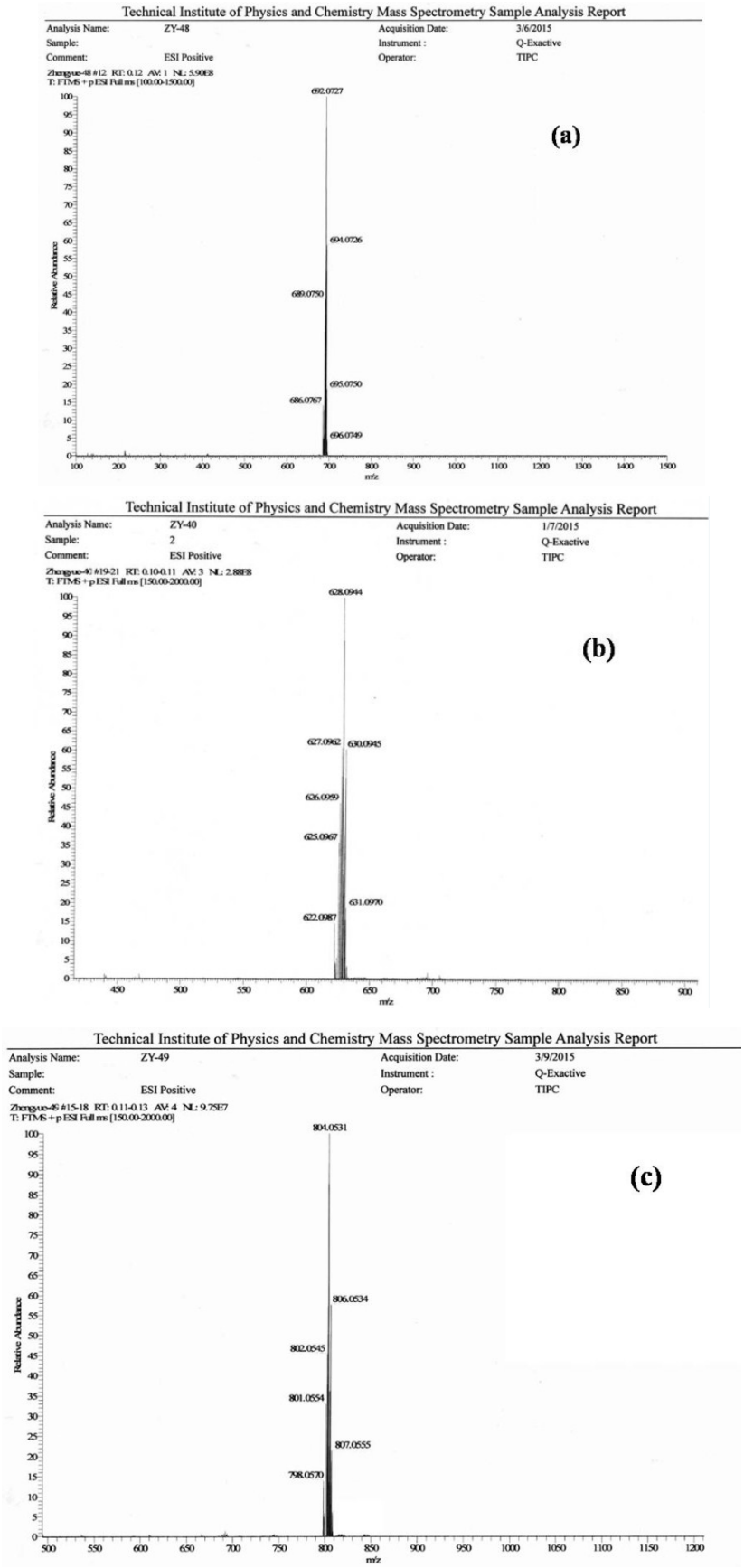

Figure S24. HR ESI-MS spectra of **1** (a), **2** (b), and **4** (c) in CH_3CN.

References

1. M. Kepczynski, R. P. Pandian, K. M. Smith; and B. Ehrenberg, *Photochem. Photobiol.* 2002, **76**, 127-134.
2. M. J. Frisch, G. W. Trucks, H. B. Schlegel, G. E. Scuseria, M. A. Robb, J. R. Cheeseman, G. Scalmani, V. Barone, B. Mennucci, G. A. Petersson, H. Nakatsuji, M. Caricato, X. Li, H. P. Hratchian, A. F. Izmaylov, J. Bloino, G. Zheng, J. L. Sonnenberg, M. Hada, M. Ehara, K. Toyota, R. Fukuda, J. Hasegawa, M. Ishida, T. Nakajima, Y. Honda, O. Kitao, H. Nakai, T. Vreven, J. A. Montgomery Jr., J. E. Peralta, F. Ogliaro, M. Bearpark, J. J. Heyd, E. Brothers, K. N. Kudin, V. N. Staroverov, R. Kobayashi, J. Normand, K. Raghavachari, A. Rendell, J. C. Burant, S. S. Iyengar, J. Tomasi, M. Cossi, N. Rega, J. M. Millam, M. Klene, J. E. Knox, J. B. Cross, V. Bakken, C. Adamo, J. Jaramillo, R. Gomperts, R. E. Stratmann, O. Yazyev, A. J. Austin, R. Cammi, C. Pomelli, J. W. Ochterski, R. L. Martin, K. Morokuma, V. G. Zakrzewski, G. A. Voth, P. Salvador, J. J. Dannenberg, S. Dapprich, A. D. Daniels, Ö. Farkas, J. B. Foresman, J. V. Ortiz, J. Cioslowski, D. J. Fox, *Gaussian 09*, revision A.1, Gaussian, Inc., Wallingford, CT, **2009**.
3. (a) A. D. Becke, *J. Chem. Phys.,* 1993, **98**, 5648-5652; (b) C. Lee, W. Yang and R. G. Parr, *Phys. Rev. B: Condens. Matter*., 1988, **37**, 785-789.
4. L. E. Roy, P. J. Hay and R. L. Martin, *J. Chem. Theory Comput.,* 2008**, 4**, 1029-1031.
5. (a) P. C. Harihara and J. A. Pople, *Theor. Chim. Acta*, 1973, **28**, 213-222; (b) M. M. Francl, W. J. Pietro, W. J. Hehre, J. S. Binkley, M. S. Gordon, D. J. Defrees and J. A. Pople, *J. Chem. Phys.,* 1982, **77**, 3654-3665.